

On the actual spatial resolution of Brillouin Imaging

S. Caponi¹, D. Fioretto², M. Mattarelli^{2, a)}

¹*Istituto Officina dei Materiali, National Research Council (IOM-CNR), Unit of Perugia, c/o Department of Physics and Geology, University of Perugia, Via A. Pascoli, I-06123 Perugia, Italy*

²*Department of Physics and Geology, University of Perugia, Via A. Pascoli, I-06100 Perugia, Italy*

The comprehension of the behavior of complex heterogeneous materials as the biological ones requires the adoption of imaging techniques and the analysis of spatially resolved properties. A key parameter is the spatial resolution, which depends both on the control of the probe and on the physical mechanism of interaction with the sample. In particular, in Brillouin Spectroscopy the control of the scattering volume is only one of the aspects that determine the spatial resolution, the other being the propagation of the detected vibrational modes. The simultaneous measure of the spatial resolution achieved in Brillouin and Raman Scattering processes varying the optical conditions and testing systems with different phonon propagation length provides evidence that the phonons' contribution to the resolution can be dominant and it is indeed inversely related with the optical focusing.

THE MANUSCRIPT

In a peculiar manifestation of Heisenberg Uncertainty Principle, when focusing by a lens a collimated light beam, the increased spatial definition is obtained at the expense of the definition in the light wavevector¹. This is usually of no concern in many microscopy techniques where the signal is scarcely affected by the direction of the exciting light, and even near-field excitation, where the light wavevector is practically undefined, has been effectively exploited. However, this is not the case for Brillouin Spectroscopy (BS). As a matter of fact, in its standard configuration BS is sensitive to the spontaneous (i.e. thermally activated) acoustic vibrations which are present in any material. Between all these vibrations (often called, even if improperly, “phonons”), the scattering configuration (wavevector and polarization of the exciting and collected light) selects by conservation laws, a subset of phonons whose properties are reflected on the measured spectrum (Details can be found in many books and recent reviews, e.g.²⁻⁶). In particular, in the usual description of a visco-elastic medium, Brillouin spectra present a peak whose position (ω_B) and width (2Γ) are proportional to the sound velocity V and longitudinal

^{a)} Author to whom correspondence should be addressed. Electronic mail: maurizio.mattarelli@unipg.it

The following article has been submitted to Applied Physics Letters. After it is published, it will be found at <https://aip.scitation.org/journal/apl>.

viscosity η_L , respectively. ($V = \omega_B/q; \eta_L/\rho = 2\Gamma/q^2$, q being the exchanged wavevector and ρ the density of the medium). The need for the mechanical characterization of elastically heterogeneous materials has led to development of confocal Brillouin microscopes, where the use of high NA objectives and dedicated optical configurations allows the reduction of the scattering volume down to the sub-micrometer scale. On the other hand, the use of high NA objectives has important implications on Brillouin measurements, due to the wide range of involved scattering wavevectors.

Figure 1 presents the distribution of wavevectors collected by a micro-Brillouin experiment in two different “backscattering” configurations, corresponding to the use of microscope air objectives with low (0.3) and high (0.9) NA as exemplified in the cartoon of Figure 1 a). In the computation, a homogeneous incoming beam covering all of the objective aperture and an isotropic scattered radiation were considered. Figure 1 b), shows that the NA increase leads to a significant spread in $|q|$. Using the 0.9 NA objective, the average value of $|q|$ is about 10% lower than the nominal one for the backscattering configuration. Moreover, a huge effect of NA on the angular distribution of the collected wavevectors is reported in Fig.1c: the deviation θ from the axis is important, reaching an average value of 8.5° for the low NA objective and 32° for the high NA one ($\sim \arcsin(\text{NA})/2$).

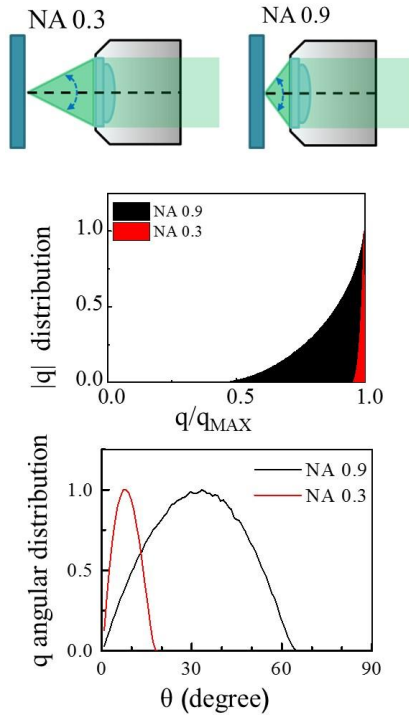


Figure 1. q distribution of the collected signal for a Brillouin scattering process in two different “backscattering” configurations exemplified in the upper cartoons for two NAs. The red and black curves represent the q distribution of the modulus, b), and of the angular deviation from the axis c) for $NA=0.3$ and $NA=0.9$, respectively.

The q -distribution has two main effects on the Brillouin spectra: on one hand, it lowers the spectral definition, due to the fact that both the frequency and the width of the peak depend on $|q|$ ⁷⁻⁹. In this case, a straightforward, though delicate, deconvolution procedure can be applied to extract the relevant material parameters¹⁰. On the other hand, the q -distribution implies also a distribution in the investigated directions, which in $NA=0.9$ optics can reach up to 65° from the axis. This is not relevant in homogeneous isotropic samples, but it becomes a fundamental issue when analyzing heterogeneous samples, i.e. just the ones where Brillouin imaging is of interest. In fact, given the propagating nature of the vibrations detected by BS, the q distribution translates into a lateral broadening of the investigated region. This effect can be a priori estimated considering the mean free path of acoustic phonons, L_2 . (see Figure 2)

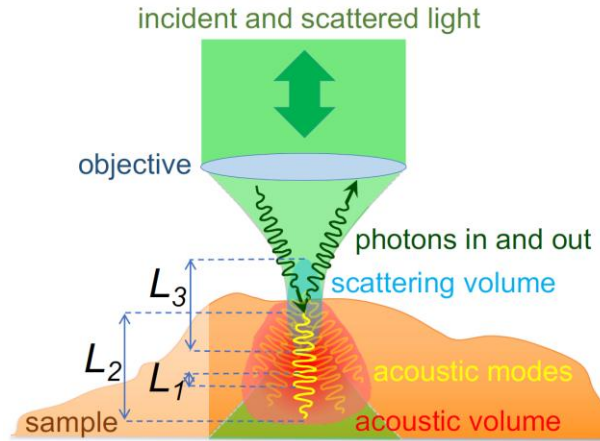


Figure 2. Schematic micro-Brillouin scattering diagram. L_1 , L_2 and L_3 denote the relevant length scales for this interaction, given by phonon wavelength, mean free path and scattering volume, respectively. The acoustic volume, in red, takes into account the broadening induced by the phonon propagation.

In principle, in a lossless homogeneous material such length is infinite. In real systems L_2 is finite because of dissipative mechanisms, be they due to static reasons, such as elastic heterogeneities on the scale of the phonon wavelength ($L_1=2\pi/q\sim 200$ nm for 532 nm lasers in backscattering) or dynamic ones such as relaxation processes¹¹⁻¹⁴. Note that both kind of mechanisms are present in biological materials and affect their Brillouin spectra^{5,15,16}. BS provides a quite effective way to measure L_2 : in fact, the peak width is inversely proportional to the phonon life time, and knowing the acoustic velocity from the Brillouin peak position it is possible to obtain L_2 from the quality factor of the peak: $L_2 = \omega_B / 2\Gamma L_1$ ¹⁷. Just as an example, the propagation length of the phonon detected in backscattering configuration by a 532 nm laser light scattered by pure water is expected to be $L_2 \sim 2.1$ μm .

A rough evaluation of the consequences of phonon propagation on micro-Brillouin spatial resolution can be obtained considering the contribution to the lateral resolution broadening arising from the average projection of L_2 by the off-axis angle, $\langle \sin(\theta) L_2 \rangle$. From the previous calculations, this effect corresponds to a lateral broadening of 0.3 and 1.1 μm , respectively, for our two NAs in water. The actual Brillouin resolution will be then given by a spatial convolution of this contribution with the scattering volume individuated by the optical system, whose lateral size is 0.7 and 0.2 μm for diffraction limited optics, respectively.

The following article has been submitted to Applied Physics Letters. After it is published, it will be found at <https://aip.scitation.org/journal/apl>.

In order to substantiate these considerations with experimental data, we measured Brillouin spectra across a sharp interface between different materials, recording the change in intensity of the Brillouin peaks. This procedure allows reconstructing the Edge Spread Function (ESF), from which we can obtain the spatial resolution of the technique¹⁰.

In particular, we analyzed two different interfaces: (i) between Polyethylene (PET) and Glycerol and (ii) between a sodium-silicate glass and water (Fig.3a). The choice of these two couples of materials was dictated by their relatively small refractive index mismatch and, more important, by their very different acoustic mismatch, so providing a direct verification of the effect of the phonon propagation on the resolution. In fact, we can expect that acoustic propagation is stopped (reflected) at the glass-water interface, while it is scarcely hindered at the PET-Glycerol interface, characterized by a lower acoustic mismatch. As the determination of the spatial resolution of the measurement can be affected by the sharpness of the interface, we carefully prepared the sample with optically polished interfaces, parallel to the optic axis. Moreover, in order to discriminate between optic and acoustic contributions to the ESF, we exploited the unique characteristics of our Raman-Brillouin combined set-up¹⁸ and simultaneously measured the ESF by both Brillouin and Raman Spectra (RS). Raman spectroscopy in fact, being related to the detection of non propagating optical phonons, can represent a good proxy for the optic contribution to the ESF as detected by the transition from one to the other material within the scattering volume.

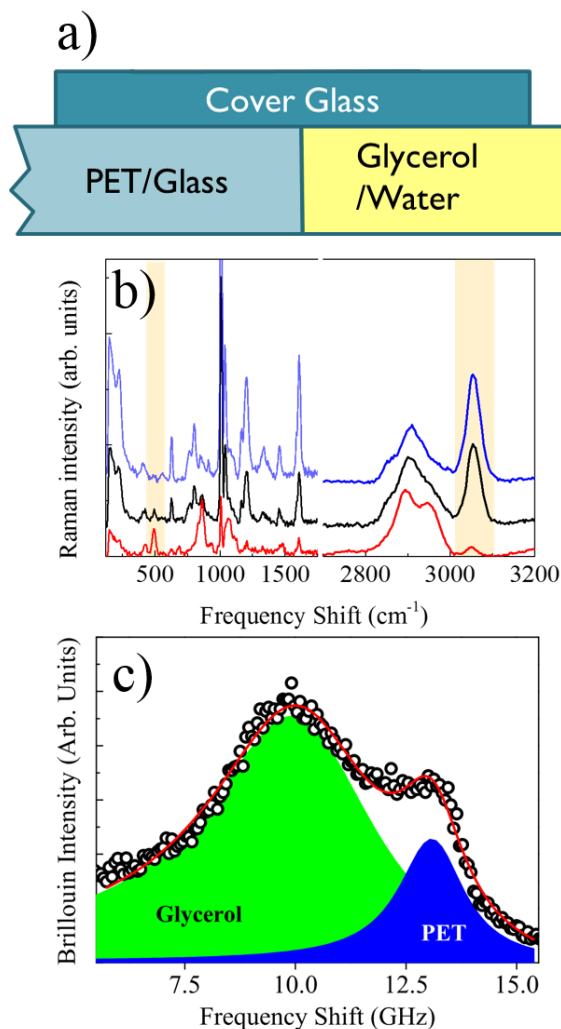


Figure 3- a) Experimental configuration; b) Evolution of the Raman spectra through the PET-Glycerol interface. The peaks located at $\sim 500 \text{ cm}^{-1}$ and $\sim 3050 \text{ cm}^{-1}$ are respectively selected to evaluate the glycerol and the PET presence in the scattering volume; c) Typical Brillouin spectrum at the PET-Glycerol interface. The experimental points were fitted by two DHO functions.

Two different objectives were used in order to change the excitation/collection configuration: a 20X NA 0.42 and a 60X water immersion objective with 1.2 NA. Note that the angular spreads of these objectives when evaluated in materials with a refractive index ~ 1.4 , as the ones we are considering, match those of the objectives NA=0.3 and NA=0.9 in air, which were previously shown in figure 1.

Several linear scans through the interface were analyzed for the two samples. As an example, in figure 3b) we show the evolution of Raman spectra acquired in the PET-Glycerol sample (figure 3a). Moreover, in Figure 3c reports the Brillouin spectrum acquired at the interface together with its fitting curve. In detail, the Brillouin spectra were analyzed using the sum of two DHO peaks as fit functions, keeping fixed the position and width of the peaks as determined from measurement on a pure material, and allowing only the intensity to vary. For the Raman spectra few well separated characteristic peaks were used to estimate the materials presence.

The intensity of the peaks, both Brillouin and Raman, changes abruptly across the interface. In Figure 4a and Figure 4b the results obtained for the two investigated interfaces with the 60X objective are reported together with the fit obtained by an error function, which allows the measure of the resolution, evaluated as two times the standard deviation σ of the corresponding Gaussian function (shown in the inset of the figures).

Figure 4 c) d) report the resolutions for the two couples of materials and for the two optical setups obtained from Brillouin and Raman measurements. The lateral width of the exciting spot, as measured by the reflected optical image when focused on an optically polished silicon wafer, is also indicated ¹⁰. The Raman resolution $2\sigma_R$ appears equal or slightly larger than the spot width, indicating that the surfaces on these length scales even if not perfectly defined give only a small contribution to the measured resolution. What is striking is the different behavior when changing the numerical aperture of the objective. While the Raman resolution follows strictly the laser spot size (with some additional contributions from the surface especially in the glass-water interface), the behavior of the Brillouin resolution $2\sigma_B$ strongly depends on the couple of interfaced materials. For the glass-water interface, the difference in the Brillouin peak frequency is $\sim 25\text{GHz}$, much larger than peak linewidths, so that no phonon present in one material can propagate into the other one. Here Brillouin and Raman techniques give the same values for spatial resolution. On the contrary, the Brillouin spectra of PET and Glycerol have a large region of superposition (Fig.2c) indicating that the phonons can propagate across the interface. Indeed, this causes a very counterintuitive effect on the measured resolution as, when reducing the scattering volume, the lateral resolution in the measure of the acoustic properties becomes worse than for the low NA objective ($1.4\ \mu\text{m}$ against $1.0\ \mu\text{m}$).

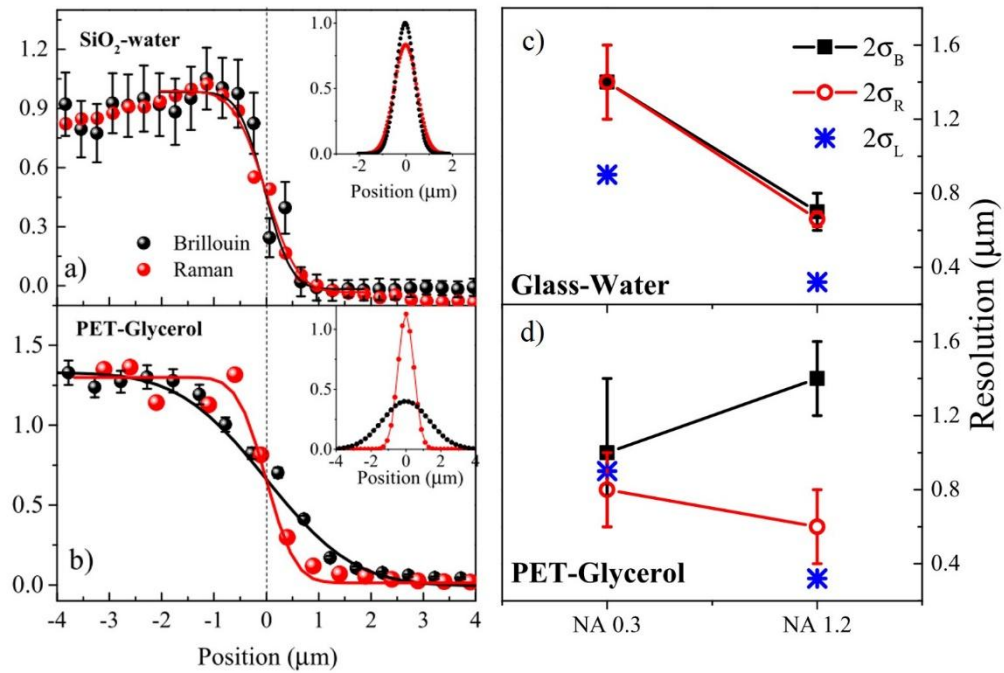


Figure 4 Rescaled PSF measured for Raman (red) e Brillouin (black) experiments through the glass-water interface a) and through the PET-Glycerol interface b). The dots are the experimental data and the lines are the fits. In the insets: Derivative of the fitting functions providing the lateral resolution of the experimental setup. c) Resolution (Brillouin, Raman, Si Reflectance indicated by black, red and blue dots, respectively) obtained from the fit of the ESF on the two interfaces (Glass –Water and PET/Glycerol) in the two optical configurations (20X NA 0.3, 60X NA 1.2))

A further confirm can be obtained by the comparison of the experimental results with previously reported calculations. In fact, the Brillouin resolution, as previously discussed, depends on the convolution of the scattering volume with the acoustic resolution, $2\sigma_E$, which is only due to the phonon propagation. Using for the lateral dimension of the scattering volume the resolution $2\sigma_R$ measured by Raman spectra and considering as a first approximation that the contributions to the spatial resolution add in quadrature (exact for Gaussian distributions), then the lateral acoustic resolution can be found as $2\sigma_E = 2\sqrt{(\sigma_B)^2 - (\sigma_R)^2}$. While this value is utterly negligible in the glass-water interface, in the PET-Glycerol interface studied by 1.2 NA objective $2\sigma_E$ is (1.2 ± 0.4) μm, indeed the dominating term in the final resolution. This value should be compared with the average

The following article has been submitted to Applied Physics Letters. After it is published, it will be found at <https://aip.scitation.org/journal/apl>.

radial projection of mean free path L_2 along the angle θ . L_2 can be estimated from the Brillouin spectra as $L_2 = \omega_B/2\Gamma L_1$, which is $\sim 2.5 \mu\text{m}$ for PET and $\sim 1.6 \mu\text{m}$ for Glycerol, and the average $\sin(\theta)$ from the angular q distribution (figure 1,c) (~ 0.52 for the 1.2 NA objective). The calculated value for $2\sigma_E$ thus falls in the range $0.8 - 1.3 \mu\text{m}$, in good agreement with the experimental value.

The present analysis is of significant relevance for a critical assessment of a number of recent works^{10,19-23}, where submicrometric features are discriminated on the basis of Brillouin signature. While the comparison with different optical techniques indicates that the observed elastic modulation is indeed related to structural changes, the measured values of the elastic constant should be considered as spatial averages, whose extent depends on both NA of the optics and on the propagation length of phonons, in turn depending on the investigated material. As a consequence, the optimization of the resolution can require the adoption of lower NA optics. For example, in a recent work²³, a reduction in the elastic contrast was observed for NA= 0.85 with respect to NA= 1.28. Our present work suggests a contribution to the different lateral resolutions coming from acoustic resolution, which is expected to be ~ 0.3 and $\sim 0.6 \mu\text{m}$, for the two objectives, respectively.

Finally, it is important to highlight the strong influence of interfaces (i.e. abrupt changes of acoustic impedance) on the phonon propagation and therefore on the elastic resolution. In presence of phonon confinement in three dimensions as in nanoparticles or in one as in films, acoustic vibrations, standing in the confined direction, are present. In this case, the spatial resolution in the measurements of the elastic properties can be even higher than the optical resolution.^{3,24-27}

In conclusion, we have shown that the ultimate resolution in the mechanical properties attainable by Brillouin imaging is limited not by the optical system but by the propagation properties of the investigated elastic waves. As a matter of fact, in Brillouin spectroscopy phonons and not light are the probe of the mechanical properties of the material. The light (according to the scattering geometry) only allows selecting the range of phonons by which we interrogate the material. The selection is in frequency by the $|q|$ spread, in direction by the angle distribution of q , and spatially by the scattering volume. However, the spatial resolution depends not only on the dimension of the scattering volume, but also on the mean free path L_2 of acoustic phonons, modulating the refractive index inside the scattering volume, which can extend over a much larger space. As a consequence, the

The following article has been submitted to Applied Physics Letters. After it is published, it will be found at <https://aip.scitation.org/journal/apl>.

actual elastic resolution can indeed get worse when increasing the optical resolution (the NA). Note that this is an inescapable constraint arising from the very fundamental reason that the detected excitations are travelling acoustic waves.

REFERENCES

- ¹ E.H.K. Stelzer and S. Grill, *Opt. Commun.* **173**, 51 (2000).
- ² B.J. Berne and R. Pecora, *Dynamic Light Scattering: With Applications to Chemistry, Biology, and Physics* (Wiley-Interscience, New York, NY (USA), 1976).
- ³ G. Carlotti, *Appl. Sci.* **8**, 124 (2018).
- ⁴ R. Prevedel, A. Diz-Muñoz, G. Ruocco, and G. Antonacci, *Nat. Methods* **16**, 969 (2019).
- ⁵ F. Palombo and D. Fioretto, *Chem. Rev.* **119**, 7833 (2019).
- ⁶ K. Elsayad, S. Polakova, and J. Gregan, *Trends Cell Biol.* **29**, 608 (2019).
- ⁷ A. Battistoni, F. Bencivenga, D. Fioretto, and C. Masciovecchio, *Opt. Lett.* **39**, 5858 (2014).
- ⁸ G. Antonacci, M.R. Foreman, C. Paterson, and P. Török, *Appl. Phys. Lett.* **103**, 221105 (2013).
- ⁹ R. Shaashoua, I. Remer, and A. Bilenca, in *Front. Opt. + Laser Sci. APS/DLS* (OSA, Washington, D.C., 2019), p. JTU4A.97.
- ¹⁰ S. Mattana, M. Mattarelli, L. Urbanelli, K. Sagini, C. Emiliani, M.D. Serra, D. Fioretto, and S. Caponi, *Light Sci. Appl.* **7**, 17139 (2018).
- ¹¹ S. Caponi, S. Corezzi, M. Mattarelli, and D. Fioretto, *J. Chem. Phys.* **141**, 214901 (2014).
- ¹² M. Mattarelli, M. Montagna, T. Still, D. Schneider, and G. Fytas, *Soft Matter* **8**, 4235 (2012).
- ¹³ S. Caponi, P. Benassi, R. Eramo, A. Giugni, M. Nardone, A. Fontana, M. Sampoli, F. Terki, and T. Woignier, *Philos. Mag.* **84**, 1423 (2004).
- ¹⁴ W.M. Du, G. Li, H.Z. Cummins, M. Fuchs, J. Toulouse, and L.A. Knauss, *Phys. Rev. E* (1994).
- ¹⁵ R. Mercatelli, S. Mattana, L. Capozzoli, F. Ratto, F. Rossi, R. Pini, D. Fioretto, F.S. Pavone, S. Caponi, and R. Cicchi, *Commun. Biol.* **2**, 1 (2019).
- ¹⁶ S. Mattana, S. Caponi, F. Tamagnini, D. Fioretto, and F. Palombo, *J. Innov. Opt. Health Sci.* **10**, 1742001 (2017).
- ¹⁷ R. Vacher, J. Pelous, and E. Courtens, *Phys. Rev. B - Condens. Matter Mater. Phys.* **56**, R481 (1997).
- ¹⁸ F. Scarponi, S. Mattana, S. Corezzi, S. Caponi, L. Comez, P. Sassi, A. Morresi, M. Paolantoni, L. Urbanelli, C. Emiliani, L. Roscini, L. Corte, G. Cardinali, F. Palombo, J.R. Sandercock, and D. Fioretto, *Phys. Rev. X* **7**, 1 (2017).
- ¹⁹ G. Antonacci, V. de Turrís, A. Rosa, and G. Ruocco, *Commun. Biol.* **1**, 139 (2018).
- ²⁰ G. Scarcelli, W.J. Polacheck, H.T. Nia, K. Patel, A.J. Grodzinsky, R.D. Kamm, and S.H. Yun, *Nat. Methods* **12**, 1132 (2015).
- ²¹ A. Karampatzakis, C.Z. Song, L.P. Allsopp, A. Filloux, S.A. Rice, Y. Cohen, T. Wohland, and P. Török, *Npj Biofilms Microbiomes* **3**, 20 (2017).
- ²² D. Fioretto, S. Caponi, and F. Palombo, *Biomed. Opt. Express* **10**, 1469 (2019).
- ²³ C. Bevilacqua, H. Sánchez-Iranzo, D. Richter, A. Diz-Muñoz, and R. Prevedel, *Biomed. Opt. Express* **10**, 1420 (2019).
- ²⁴ T. Still, M. Mattarelli, D. Kiefer, G. Fytas, and M. Montagna, *J. Phys. Chem. Lett.* **1**, 2440 (2010).
- ²⁵ D. Schneider, P.J. Beltramo, M. Mattarelli, P. Pfeleiderer, J. Vermant, D. Crespy, M. Montagna, E.M. Furst, and G. Fytas, *Soft Matter* **9**, 9129 (2013).
- ²⁶ A. Girard, J. Margueritat, L. Saviot, D. Machon, B. Mahler, M.D. Tessier, S. Pedetti, B. Dubertret, H. Géhan, E. Jeanneau, R. Vera, and A. Mermet, *Nanoscale* **9**, 6551 (2017).
- ²⁷ M. Mattarelli and M. Montagna, *Chem. Phys. Lett.* **524**, 112 (2012).